Stephan Bansmer (Autor)

Aircraft icing

A challenging problem of fluid mechanics.

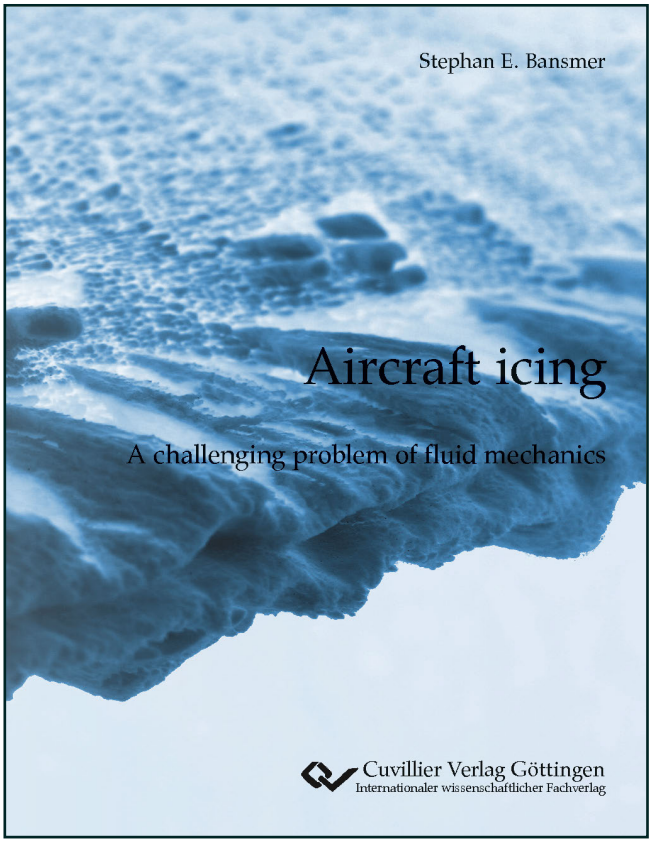

https://cuvillier.de/de/shop/publications/8249

1
Historical remarks and current airframer perspectives on icing

With the growing need for scheduled flights under all weather conditions since the 1920s, the subject of aircraft icing involves nearly one century of research, technology development and cross-fertilization over different engineering disciplines. Without being exhaustive, the timeline on page 15 identifies major milestones and knowledge drivers as well as accidents and failures that form the current view of aircraft icing. This chapter summarizes these developments and provides information on current certification aspects for flight in icing conditions.

1.1 Milestones in icing research

The 1920s and 1930s can be considered the dawn of modern aviation. In aircraft design, anodized aluminium replaced wooden structures. Pioneers like Albert Read, Charles Lindbergh and Charles Kingsford Smith crossed the oceans. Carriers like *Koninklijke Luchtvaart Maatschappij (KLM)* and *Deutsche Luft Hansa* were founded. The demand for scheduled day-and-night flight operations grew rapidly. Soon, aircraft icing was recognized as a great obstacle. To circumvent ice accretion on the leading edge of the wings, pneumatic boots were developed for de-icing; a Northrop Alpha mail plane was the first commercial aircraft equipped with rubber blankets from Goodrich. A good summary of the earliest research on aircraft icing can be found in the Russian literature.[1]

During World War II, much theoretical work on ice accretion was performed by the Nobel laureate Irving Langmuir. Perhaps stimulated by his experience as a private pilot but also motivated by the US Army Air Forces, Langmuir studied electrostatic precipitation on aircraft flying through snowstorms, the supercooling of droplets and ice adhesion on metal surfaces.[2] By combining his mathematical theory on droplet trajectories with data on cylinder ice accretion gathered on Mount Washington, he eventually developed a pioneer-

[1] Nikolai V. Lebedev. *Combating ice on aircraft*. State publishing house of defense industry, People's Commissariat of Aviation Industry, 1939

[2] Irving Langmuir. *The collected works of Irving Langmuir*, volume 10. Pergamon Press, 1961

ing method for establishing cloud droplet sizes and their liquid water content.

THE DEBUT of the de Havilland Comet in 1952 ushered in a new era of jet airliners. Thermal ice protection systems using the bleed air of jet engines became standard. However, enormous heat requirements[3] of more than 10 percent bleed air were predicted, precluding continuous heating operation. It was Bernhard Messinger from Lockheed Aircraft Corporation who suggested in his seminal paper[4] in 1953 the design of cyclic thermal de-icing systems based on a thorough analysis of the heat and mass balances of ice accretion. However, the first studies were limited to simple geometries, such as cylinders, for which analytical solutions were deducible. The technology development thus still relied on rig tests in icing wind tunnels. The major icing wind tunnels of that time were NASA's Icing Research Tunnel[5] and the NRC's Low Speed Icing Tunnel.

INTEGRATED CIRCUITS in the 1960s and microprocessors like Intel's 4004, which was commercially launched in 1971, enabled breakthroughs in the vast and growing fields of electronics and computers. Figure 1.1 shows the exponential increase in computational power over the period of seventy years in which the field of computational fluid dynamics evolved from solvers of linear potential equations to Euler equations in the 1980s. During that time, cooperation among NASA, RAE and ONERA resulted in the first generation of icing codes[6] that incorporated much of the earlier theoretical work of LANGMUIR and MESSINGER. NASA's LEWICE code is one of these ice prediction tools that remains the standard in many industrial fields. After the end of the Cold War, many other agencies joined icing research activities, and a vast number of icing codes emerged that took advantage of solving the Reynolds-averaged Navier-Stokes equations for improved boundary layer predictions. The AGARD advisory report 344 summarizes the status of ice accretion simulation as of 1997.[7]

PARALLEL TO THIS COMPUTATIONAL PROGRESS, developments in LASER and digital image recording enriched experimental icing research. The introduction of phase Doppler interferometry for particle sizing in 1984 laid the foundations for more accurate characterizations of atmospheric icing conditions and icing wind tunnel experiments. As a consequence, details of the icing process came into focus in experimental studies. The visualization of ice roughness growth by OLSEN and WALKER (1986) and investigations on water film dynamics during ice accretion by MYERS and HAMMOND (1999) are just a

[3] Thomas F. Gelder, James P. Lewis, and Stanley L. Koutz. Icing Protection for a Turbojet Transport Airplane: Heating Requirements, Methods of Protection, and Performance Penalties. Technical Report NACA-TN-2866, National Advisory Committee for Aeronautics, 1953

[4] Bernard L. Messinger. Equilibrium temperature of an unheated icing surface as a function of air speed. *Journal of the Aeronautical Sciences*, 20(1): 29–42, 1953

[5] William M. Leary. "We Freeze to Please": A History of NASA's Icing Research Tunnel and the Quest for Flight Safety. Technical Report NASA/SP-2002-4226, National Aeronautics and Space Administration, 2002

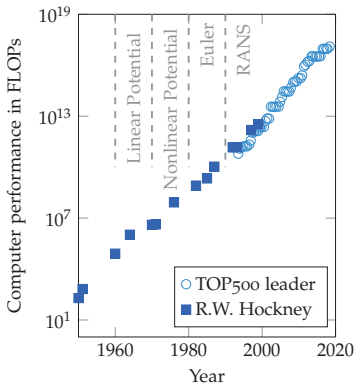

Figure 1.1: Development of computational performance over the last 70 years. Chronology of computational methods for fluid dynamics in ANTONY JAMESON's view.

[6] Roger W. Gent, Nicholas P. Dart, and James T. Cansdale. Aircraft icing. *Philosophical Transactions of the Royal Society of London A: Mathematical, Physical and Engineering Sciences*, 358 (1776):2873–2911, 2000

[7] Bernhard Wagner. Ice Accretion Simulation. Technical Report AGARD report no. 344, North Atlantic Treaty Organization, 1997

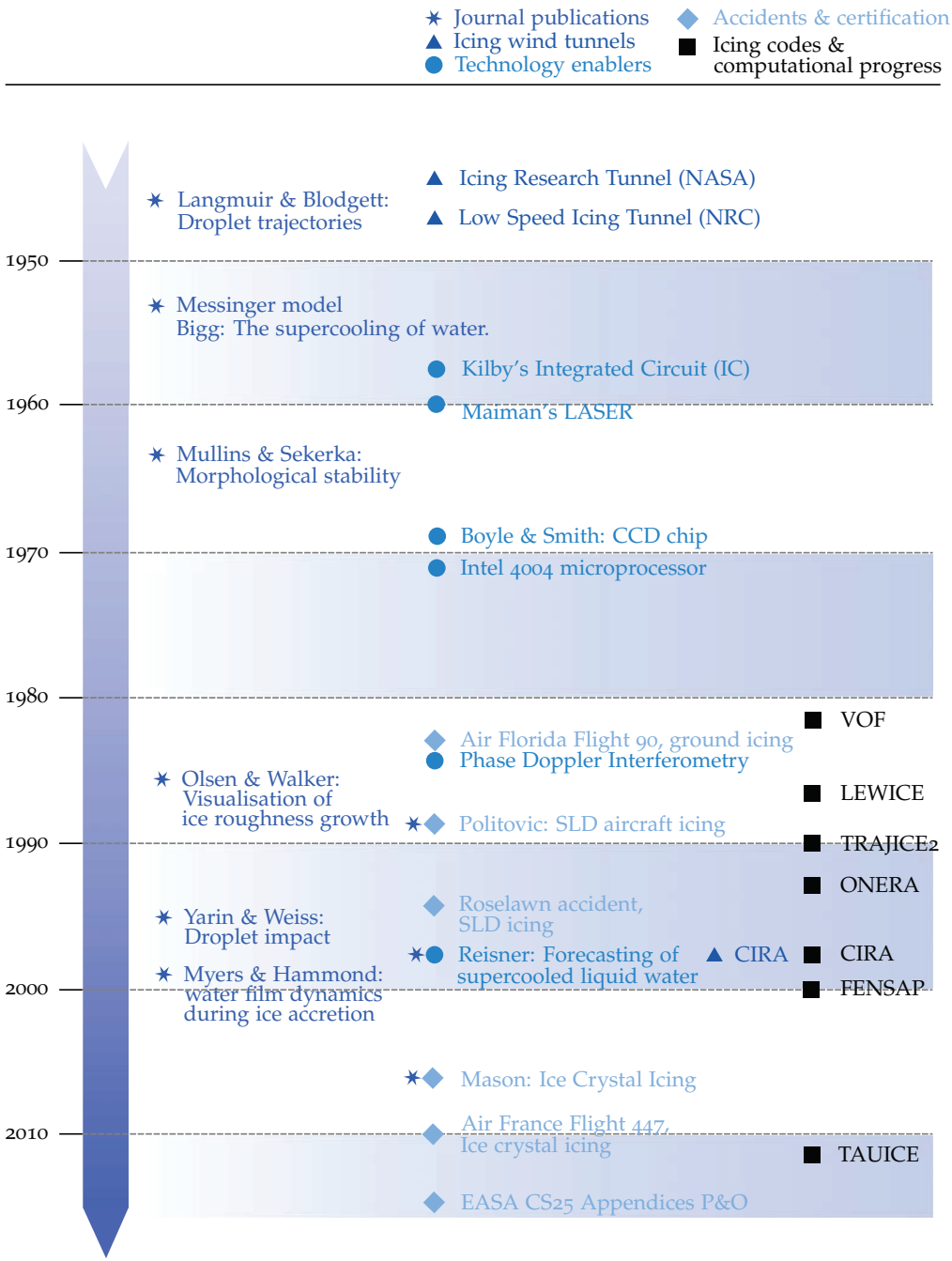

Figure 1.2: A glimpse of scientific publications, technology enablers, drivers and developments that shaped the field of modern icing research.

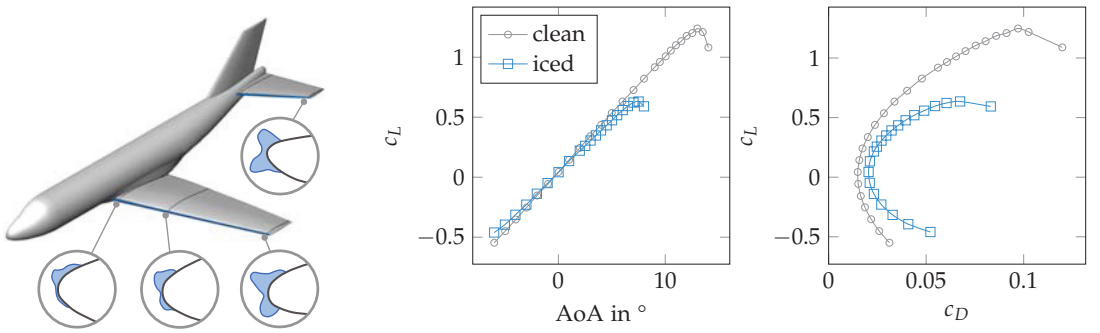

Figure 1.3: Half-model of the VFW 614 ATTAS aircraft including simulated leading edge ice accretion on the main wings and horizontal tail plane. The aerodynamic performance is significantly deteriorated compared with that of the clean configuration. Adapted picture and data from DEILER and KILIAN (2018).

few examples. The new findings improved the underlying computational models, although further improvements are an ongoing effort in the aircraft icing community.

1.2 *Certification of commercial transport aircraft*

Before entering into operation, a newly developed aircraft model must obtain a type certificate issued by the responsible aviation regulatory authority. These agencies include the Civil Aviation Directorate in Canada, the Federal Aviation Administration (FAA) in the US, and the European Aviation Safety Agency (EASA) in Europe. Depending on the aircraft type, specific guidelines for certification are applicable to demonstrate compliance with the regulatory requirements. For large transport aircraft in Europe, the EASA CS-25 document lists the certification specifications. Articles CS25.1419, CS25.1420 and CS25.1093 and appendices C, O and P are relevant for certification for flight in icing conditions. Three major icing phenomena are addressed: supercooled droplet icing, supercooled *large* droplet icing[8] and mixed phase icing.[9] The latter phenomenon was discovered only recently and encompasses ice crystals, which can become sticky on warm surfaces, like in Pitot probes and in the low-pressure compressor stages of jet engines.

BUILDING ON THE PREDICATIVE CAPABILITY of modern icing codes, the philosophy of icing certification has shifted in the last two decades from complete reliance on rig testing towards design by computational analysis. Figure 1.3 highlights the possibilities of state-of-the-art tools applied to a VFW 614 ATTAS aircraft model. In the first step, ice accretion on the wings and the horizontal tail plane is simulated using the TAUICE code. Note the different ice shapes along the wingspan, which are called glaze ice horns. The deteriorating aerodynamic performance of the configuration is evaluated with

[8] Marcia K. Politovich. Aircraft Icing Caused by Large Supercooled Droplets. *Journal of Applied Meteorology*, 28(9): 856–868, 1989

[9] Arne Baumert, Stephan E. Bansmer, Pierre Trontin, and Philippe Villedieu. Experimental and numerical investigations on aircraft icing at mixed phase conditions. *International Journal of Heat and Mass Transfer*, 123:957–978, 2018

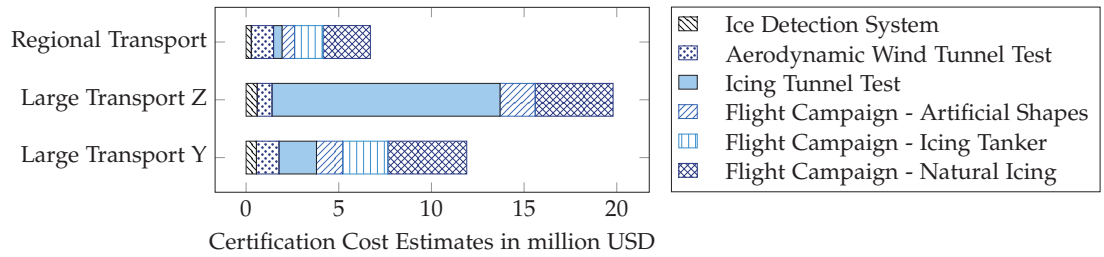

Figure 1.4: EASA Part 25 Appendix O certification cost estimates. Data source: Working group report on supercooled large droplet rulemaking.

the DLR flow solver TAU. When compared with clean conditions, the maximum lift decreases, and both the stall speed and aerodynamic drag increase. As a consequence, the flight envelope of the aircraft is significantly reduced, which poses a serious threat to flight safety, especially during the flight phase of holding and approach to landing. Details of the computational approach will be discussed in Chapter 9.

Despite computational advances, wind tunnel and flight tests are still an important pillar in the certification procedure when validation data are sparse. One example is the new requirements for compliance with supercooled large droplet (SLD) icing that were issued only recently in 2016. Due to their increased inertia, large droplets can impact and accrete further downstream in regions that might not be protected by classical anti-icing systems. The study of ice accretion is therefore always linked to the design task of ice protection systems. The power requirements of an anti-icing system are usually approximately 150 kW, regardless of the aircraft size; for small aircraft, nearly the entire leading edge must be protected, while large aircraft meet the requirements by protecting a limited number of slats. Cost estimates for the SLD-icing certification procedures from different airframers are consolidated in Figure 1.4.

Flight safety is the driving paradigm in the entire certification process. Continued progress in the fields of computational analysis and experimental testing procedures maintains high safety standards. Statistics from NASA's Aviation Safety Reporting System (ASRS) and the Bureau of Transportation Statistics (BTS) emphasize that trend, as shown in Figure 1.5. While the number of enplanements has steadily grown over recent decades, the numbers of incidents and accidents remain rather small.

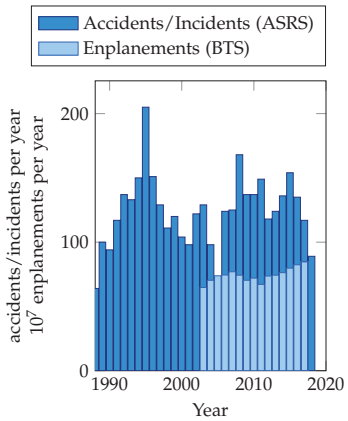

Figure 1.5: Statistics on icing incidents/accidents in the US airspace. Data sources: ASRS and BTS. Data search methodology adapted from Green (2006).

2
A challenging problem of fluid mechanics

Supercooled droplet icing is the most frequently encountered scenario for aircraft icing. It involves fluid mechanics on various time and length scales and covers fundamental problems like drop impact, turbulent flow, and non-equilibrium thermodynamics. Consequently, the definition and assessment of many boundary conditions are mandatory.

2.1 Supercooled droplet icing: phenomenology and scales

A droplet is called supercooled when it is in liquid phase but its temperature is below the freezing point. The lifetime of this metastable state varies from a few seconds to several days, depending on the droplet's size and the difference in temperature from the equilibrium freezing point at 0 °C.[1] Minor perturbations can initiate the phase change. Hence, the drop solidifies upon impact onto a solid substrate, which is the basis of ice accretion.

[1] Hans R. Pruppacher. A new look at homogeneous ice nucleation in supercooled water drops. *Journal of the Atmospheric Sciences*, 52(11):1924–1933, 1995

The temporal evolution of ice accretion on an NACA0012 aerofoil is visualized in Figure 2.1. At $t_{acc} = 0$, the initially dry aluminium aerofoil is exposed to a cloud of supercooled droplets. After five seconds, the surface is fully wetted in the vicinity of the stagnation line. A thin water film forms, whose liquid/gas interface is subject to several instability mechanisms, including the formation of

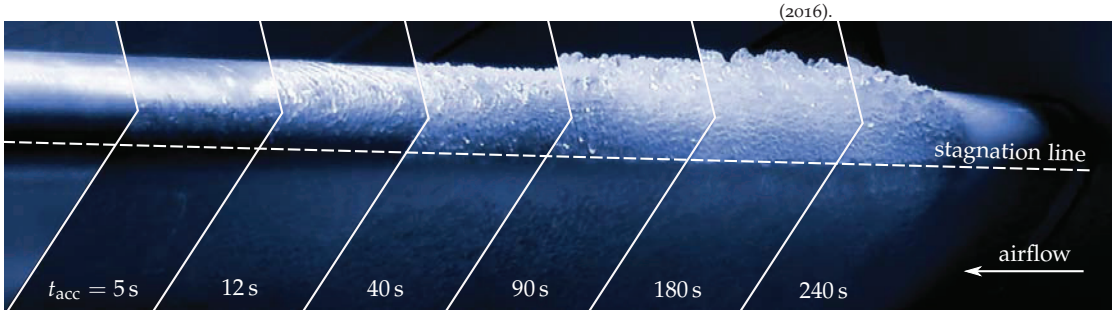

Figure 2.1: Ice accretion on an NACA0012 aerofoil over time. $T_\infty = 263.15\,K$, LWC $= 1.3\,g\,m^{-3}$, MVD $= 80\,\mu m$, AoA $= 8°$. Data from Sommerwerk, Horst and Bansmer (2016).

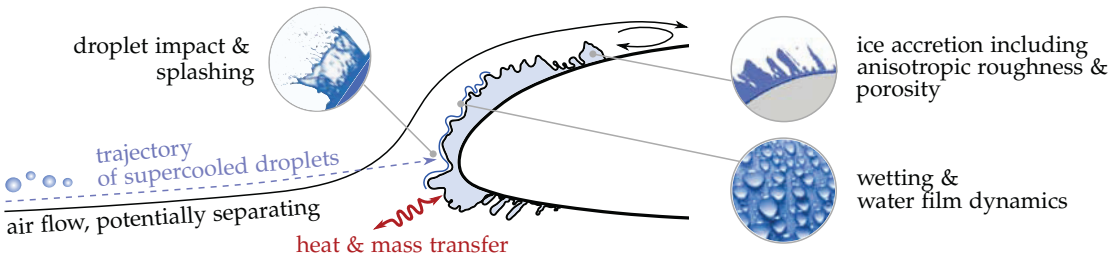

Figure 2.2: Summary of fluid mechanical phenomena associated with aircraft icing.

rivulets. Subsequently, solidification commences, and small roughness elements are formed that grow over time. Two minutes later, the accreted ice layer already has a thickness of several centimetres.

Obviously, several fluid mechanical phenomena are involved in the icing process, which are summarized in Figure 2.2. Each of these individual phenomena has attracted many researchers in the past, as reflected by the cited ground-breaking literature and Nobel laureates. The major challenges can be outlined as follows:

- **Droplet trajectories.** The gravity, aerodynamic drag, and inertia of the droplet imply trajectories[2] that deviate from the airflow streamlines. These trajectories govern the mass balance of ice accretion.
- **Droplet impact** at high velocities promotes splashing.[3] Secondary droplets are generated, which alter the local mass balance of ice accretion and might re-impinge on installations further downstream.
- **Large ice roughness**, partially wetted by thin water films.[4] Anisotropic roughness elements are observed that severely interfere with the aerodynamic boundary layer. The roughness height can vary by about one order of magnitude in the streamwise direction.
- **The laminar/turbulent flow transition** is shifted upstream due to abundant roughness elements that create large-amplitude disturbances in the region of laminar flow.[5]
- **Heat and mass transfer.** A broad range of thermodynamic processes[6] are involved in aircraft icing, particularly kinetic and viscous heating, convection, conduction, solidification and evaporation. Since the thermal and concentration boundary layers exhibit similarities to the velocity boundary layer, the aforementioned challenges of roughness and water film dynamics fully apply to the problem of heat and mass transfer.

[2] Irving Langmuir and Katherine B. Blodgett. *The collected works of Irving Langmuir*, volume 10 - Atmospheric phenomena, chapter Mathematical investigation of water droplet trajectories, pages 335–393. Pergamon press, 1961

[3] Alexander L. Yarin. Drop impact dynamics: splashing, spreading, receding, bouncing... *Annual Review of Fluid Mechanics*, 38:159–192, 2006

[4] Pyotr L. Kapitza and Sergey P. Kapitza. Wave flow of thin viscous fluid layers. *Zh. Eksp. Teor. Fiz*, 18(1): 3–28, 1948

[5] Hugh L. Dryden. Review of published data on the effect of roughness on transition from laminar to turbulent flow. *Journal of the Aeronautical Sciences*, 20(7):477–482, 1953

[6] Ilya Prigogine. *Introduction to thermodynamics of irreversible processes*. Interscience Publ., 3. ed. edition, 1967. ISBN 0470699280

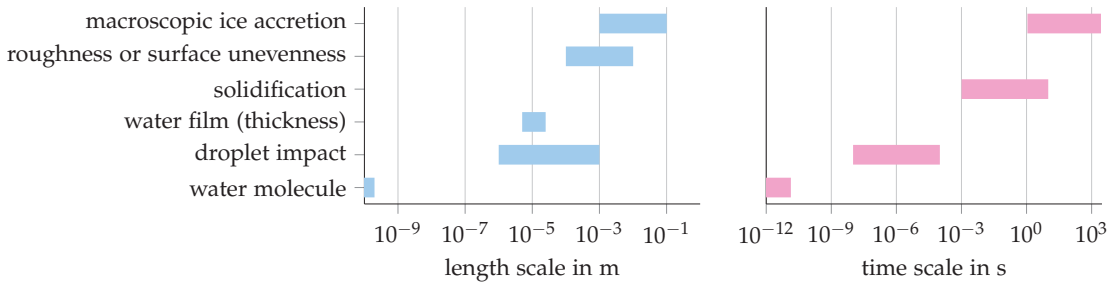

Figure 2.3: A selection of length and time scales involved in aircraft icing.

- **Flow separation.** Once a sufficient amount of ice is accumulated, the airflow might separate,[7] forming a recirculation zone behind the accretion. Simulating such detached flows is still a computational challenge.[8]

[7] Roger L. Simpson. Turbulent Boundary-Layer Separation. *Annual Review of Fluid Mechanics*, 21(1):205–232, 1989

[8] Philippe R. Spalart. Detached-eddy simulation. *Annual Review of Fluid Mechanics*, 41:181–202, 2009

Several length and time scales form the basis of ice accretion, as shown in Figure 2.3. These scales range from molecular reorientation within picoseconds during phase change to macroscopic ice growth, which can last several hours or longer. The present monograph is therefore divided into another two parts that consider the micro- and macro-scales of ice accretion separately.

2.2 *Boundary conditions and scaling laws*

The multitude of phenomena necessitate the definition of several boundary conditions. Most importantly, the airflow and droplet cloud must be characterized.

Boundary conditions for airflow

Fluid motion is governed by the conservation of mass, momentum and energy. Mathematically, this concept can be described with transport equations that are further outlined on page 86. Their analysis reveals three major physical effects relevant to icing that must be characterized with appropriate boundary conditions:

- **Inertial effects.** A body $\mathscr{B}$ moves with velocity U_∞ through a fluid with density ϱ_{air}. The body locally deflects the flow, yielding inertial forces according to Newton's second law.

- **Viscous effects.** The dynamic viscosity of air μ_{air} will mainly influence the flow inside a thin region near the surface of the body, which is called the *boundary layer*.[9]

[9] Hermann Schlichting. *Boundary-Layer theory*. Springer, Berlin, 9th edition, 2017. ISBN 9783662529171

LWC fraction *in %*	5	10	20	30	20	10	5
$\left(\frac{d}{\mathrm{MVD}}\right)^2$	0.31	0.52	0.71	1	1.37	1.74	2.22

Table 2.1: Langmuir-D distribution of droplet size.

- **Compressibility.** When the static pressure p_{air} of air increases, its density ϱ_{air} will increase. Under isentropic conditions, the relation $a_{\mathrm{air}}^2 = \frac{\partial p_{\mathrm{air}}}{\partial \varrho_{\mathrm{air}}}$ applies, where a_{air} represents the speed of sound.[10] Compressibility manifests itself at higher flow velocities, where the pressure variations around the body become large compared with the absolute pressure.

[10] John David Anderson. *Modern compressible flow*. McGraw-Hill series in aeronautical and aerospace engineering. McGraw-Hill, 3rd edition, 2003. ISBN 0071121617

Boundary conditions for the droplet cloud

The airflow is laden with a cloud of supercooled droplets, which can be characterized by the following parameters:

- Water concentration in the air, which is quantified by the **liquid water content** (LWC), a measure of the mass of water per unit volume of air. Typical values for atmospheric icing conditions range from $0.1\,\mathrm{g\,m^{-3}}$ to $3\,\mathrm{g\,m^{-3}}$.

- **Median volume diameter** (MVD) of the statistical distribution of water droplets in the liquid cloud. The MVD attempts to reduce the size distribution to a single representative scalar diameter. This idea is attributed to Langmuir.[11] His theory of droplet trajectories relates droplet size distributions and ice accretion on a cylinder. After exposing a cylinder to a cloud of super-cooled fog, Langmuir derived an assumption of the droplet size spectra, which can be found in Table 2.1. The term "median" results from the median value of the LWC in this distribution, where $d/\mathrm{MVD} = 1$. Langmuir himself described the MVD as a diameter "such that half of the liquid water content of the fog is in droplets of larger [diameter] and the other half in droplets of smaller [diameter]."

[11] Irving Langmuir and Katherine B. Blodgett. *The collected works of Irving Langmuir*, volume 10 - Atmospheric phenomena, chapter Mathematical investigation of water droplet trajectories, pages 335–393. Pergamon press, 1961; and Karen J. Finstad, Edward P. Lozowski, and Lasse Makkonen. On the median volume diameter approximation for droplet collision efficiency. *Journal of the Atmospheric Sciences*, 45 (24):4008–4012, 1988

- **Humidity**, i.e., the amount of water vapour in the air, can influence the freezing process of supercooled droplets.[12] A distinction is made between the absolute humidity (AH) and relative humidity (RH). AH is defined by the mass of water vapour per unit volume of dry air. With the partial pressure of the water vapour p_{vap}, the static temperature T_{air} of the air and the specific gas constant of the vapour $\mathscr{R}_{\mathrm{vap}}$, this definition yields $\mathrm{AH} = \frac{p_{\mathrm{vap}}}{\mathscr{R}_{\mathrm{vap}} T_{\mathrm{air}}}$. RH is defined as the ratio of the partial pressure of water vapour p_{vap} to the equilibrium vapour pressure of water $p_{\mathrm{vap}}^{\bullet}$, i.e., $\mathrm{RH} = \frac{p_{\mathrm{vap}}}{p_{\mathrm{vap}}^{\bullet}}$.

[12] Stefan Jung, Manish K. Tiwari, N. Vuong Doan, and Dimos Poulikakos. Mechanism of supercooled droplet freezing on surfaces. *Nature Communications*, 3:615, January 2012

Rime and glaze ice

Ice accretion is initiated when a cloud of supercooled droplets collides with the body $\mathscr{B}$. The **static air temperature** T_{air} governs the subsequent solidification process. At very low temperatures, the droplets will freeze shortly after their impingement and entrap the surrounding air. The resulting ice accretion is called rime ice; see Figure 2.4. As the temperature increases, the solidification process of the impacting droplets is retarded, promoting wind-driven water film dynamics. At locations with increased convective heat transfer, the water film freezes, yielding a nearly transparent glaze ice shape with typical horn formations. The list of boundary conditions is completed by the **accumulation time** t_{acc} for which the body $\mathscr{B}$ is exposed to the cloud of super-cooled droplets.

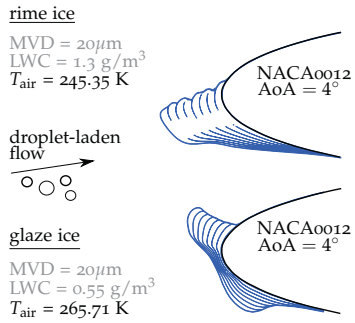

Figure 2.4: Rime ice and glaze ice shapes over time at the leading edge of an NACA0012 aerofoil, chord length 0.53 m. One blue line represents one minute of ice accretion. Further boundary conditions (rime): $U_\infty = 58\,\text{m}\,\text{s}^{-1}$, $t_{\text{acc}} = 8\,\text{min}$; (glaze): $U_\infty = 102.8\,\text{m}\,\text{s}^{-1}$, $t_{\text{acc}} = 7\,\text{min}$. Data from computations with TAUICE by Jan Steiner.

Non-dimensional groups and scaling laws

For airworthiness certification, aircraft and engine manufacturers perform many icing wind tunnel experiments with subscale models before full-scale flight tests. For such subscale tests, all the above-mentioned dimensional boundary conditions have to be adapted to produce an icing result similar to that obtained in a full-scale reference model. Furthermore, limited ranges of air speed, test section dimensions and icing cloud characteristics in the icing wind tunnels have to be contemplated. In the first step, non-dimensional groups must be deduced from the boundary conditions.[13]

[13] Thomas H. Bond and David N. Anderson. Manual of Scaling Methods. *NASA/CR-2004-212875*, 2004

Airflow similarity requires an interrelation among inertial, viscous and compressible effects. For this purpose, both the Reynolds number and Mach number are introduced:

$$\text{Re}_{\text{air}} = \frac{\varrho_{\text{air}} \cdot U_\infty \cdot d_{\text{nose}}}{\mu_{\text{air}}} \qquad \text{Ma}_{\text{air}} = \frac{U_\infty}{a_{\text{air}}} \quad .$$

Because icing mainly occurs in the vicinity of the leading edge of an aerofoil, the reference length d_{nose} in the Reynolds number definition is chosen as twice the nose radius.

The trajectories of supercooled droplets provide information on if and where a droplet will impinge on the aerofoil surface. They are hence an important element for determining the mass balance of ice accretion. Analysing the equation of droplet motion – cf. Chapter 9.3 – suggests a non-dimensional inertia parameter $\mathfrak{K}$, given by

$$\mathfrak{K} = \frac{\varrho_{\text{d}} \cdot \text{MVD}^2 \cdot U_\infty}{18 d_{\text{nose}} \cdot \mu_{\text{air}}} \quad ,$$

Method	Similarity parameters							
	Re_{air}	Ma_{air}	$\mathfrak{K}$	A_c	f_0	$\mathrm{Y_d}$	Y_{air}	Y_{rel}
Charpin and Fasso (1972)			*	*	*			*
Ruff (1986) – no. 1			*	*				
– no. 2			*	*	*			
– no. 3			*	*	*			*
– no. 4			*	*	*	*	*	*

Table 2.2: A selected number of icing similarity studies.

where ϱ_d denotes the droplet's density. The impinging mass flux of supercooled droplets is transformed into a non-dimensional accumulation parameter A_c:

$$A_c = \frac{\mathrm{LWC} \cdot U_\infty \cdot t_{acc}}{\varrho_{ice} \cdot d_{nose}} \quad .$$

Herein, ϱ_{ice} represents the density of ice.

THE ENERGY TRANSFER among air, impacting droplets, ice and water film involves many physical phenomena. See Chapter 9.4 for a detailed discussion. Many non-dimensional parameters can be derived, among which the stagnation line freezing fraction f_0 has become very popular:

$$f_0 = \frac{c_{p,ws}}{L_{fus}} \left[\mathrm{Y_d} + \frac{\mathrm{Y}_{air}}{\mathrm{Y}_{rel}} \right] \quad ,$$

where

$$\mathrm{Y_d} = 273.15\ \mathrm{K} - T_{\infty,air} - \frac{U_\infty^2}{2 c_{p,ws}}$$

$$\mathrm{Y}_{air} = T_S - T_{\infty,air} - \frac{U_\infty^2}{2 c_{p,air}} + \frac{1}{c_{p,air}} \left(\frac{\mathrm{Pr}_{air}}{\mathrm{Sc}_{air}} \right)^{\frac{2}{3}} \frac{p_{ww} - p_w}{p_{\infty,air}} L_{evap}$$

$$\mathrm{Y}_{rel} = \frac{d_{nose}}{\mathrm{Nu}_{air}\, k_{air}}\, \mathrm{LWC}\, U_\infty \beta_0 \left(\mathfrak{K}\right) c_{p,ws} \quad .$$

The stagnation line freezing fraction can be interpreted as the percentage of water at the stagnation line that will freeze. Note that the parameter Y_{rel} is dimensionless, while $\mathrm{Y_d}$ and Y_{air} have units of temperature.

$c_{p,air}$	constant-pressure specific heat of air
$c_{p,ws}$	specific heat of water on model surface
k_{air}	thermal conductivity coefficient
L_{fus}	latent heat of fusion
L_{evap}	latent heat of vaporization
p_{ww}	vapour pressure of water over liquid water
p_w	vapour pressure of water in the atmosphere
Nu_{air}	Nusselt number
Pr_{air}	Prandtl number
Sc_{air}	Schmidt number
Y_{air}	air energy transfer parameter
$\mathrm{Y_d}$	drop energy transfer parameter
Y_{rel}	relative heat factor
β_0	stagnation-line catch efficiency

THE ACCURATE SCALING of the test conditions between the reference and subscale model would require matching all the above non-dimensional groups. Merely matching the Reynolds and Mach numbers in classical aerodynamics is seldom possible. A rigorous application of all non-dimensional groups for scaling aircraft icing is therefore unfeasible. For practical considerations, the main goal for adequate scaling is to simulate the characteristic features, such as the glaze horns, in size, location, and shape. Based on systematic empirical studies, different simplifications have been introduced, e.g.,